Arabian Journal for Science and Engineering (2023) 48:16889–16905
https://doi.org/10.1007/s13369-023-08220-x

RESEARCH ARTICLE-PETROLEUM ENGINEERING

The Influence of Ionic Strength on Transport and Retention of Hydroxyapatite Nanoparticles Through Saturated Porous Media Under Reservoir Conditions

Eugene N. Ngouangna[1] · Mohd Zaidi Jaafar[1,2] · M. N. A. M. Norddin[1,2,5] · Augustine Agi[3] · Jeffrey O. Oseh[1,4] · Faruk Yakasai[1] · Stanley C. Mamah[5] · Mohanad Al-Ani[1]

Received: 27 April 2023 / Accepted: 10 August 2023 / Published online: 1 September 2023

Abstract

Nanomaterials are widely used in daily life due to their outstanding properties. Nanoparticles (NPs) will unavoidably discharge and migrate across the environment throughout their whole life cycle. The destiny and behaviour of NPs in porous media, as well as the co-transport of NPs with other contaminants, have thus received a lot of interest. Despite their environmental friendliness, hydroxyapatite nanoparticles (HAP) have been used in few EOR studies. Hence, EOR applications must include HAP transport, retention, and adsorption on rock surfaces. Salinity affects NPs behaviour in porous media and EOR applications. Particle adsorption on rock surfaces at distinct ionic strengths impacts reservoir NP movement. The effects of electrolyte solutions with monovalent cations of NaCl on HAP transport behaviour through porous media are yet to be examined. HAP was synthesised and functionalized in situ using sodium dodecyl sulphate (SDS). FTIR and XRD confirmed HAP synthesis, while zeta potential analysis was used to measure its stability. HAP was transported through sandstone cores at varied ionic strengths. The viscosity of brine was examined at varied concentrations and temperatures before utilising it in nanofluid (NF) formulations. XRD, SEM, FESEM, and EDX were utilised on sandstone cores before and after flooding to assess NP adsorption and retention. Breakthrough curves were used to access the transport and retention of HAP through sandstone. Ultimate nanoparticle (NP) recovery is reduced with increase in ionic strength. Permeability measurements before and after NP transport proved that fewer NPs were agglomerated in the rock sample. FESEM, XRD, and EDX results proved that more NPs were adsorbed on the rocks during the transit. An increase in ionic strength causes NP retention to rise, leading to a reduction in NP recovery.

Keywords HAP · NPs transport · EOR · Salinity · Adsorption

1 Introduction

Since 2008, the use of nanoparticles (NPs) for enhanced oil recovery (EOR) has drawn significant attention [1–4]. A lot of research has been done that can be broadly divided into two categories: (i) The development of "contrast-agent" type NPs to improve the detection limitations of seismic techniques for better reservoir characterisation [5], and (ii) the use of NPs

✉ Mohd Zaidi Jaafar
mzaidi@utm.my

✉ M. N. A. M. Norddin
anam@utm.my

✉ Jeffrey O. Oseh
jeffreyoseh@utm.my

[1] Department of Petroleum Engineering, Faculty of Chemical and Energy Engineering, Universiti Teknologi Malaysia, 81310 Johor Bahru, Malaysia

[2] Institute for Oil and Gas (IFOG), Universiti Technology Malaysia, 81310 Johor Bahru, Malaysia

[3] Faculty of Chemical and Process Engineering Technology, University Malaysia Pahang, 68145 Kuantan, Pahang, Malaysia

[4] Department of Petroleum Engineering, School of Engineering and Engineering Technology, Federal University of Technology, P.M.B 1526, Owerri, Imo State, Nigeria

[5] Advanced Membrane Technology Research Centre (AMTEC), Nanostructured Materials Research Group (NMRG) – MD - Frontier Materials, Universiti Teknologi Malaysia, 81310 Johor Bahru, Malaysia

as property modifiers to alter rock wettability and interfacial tension (IFT) at the oil/water interface [6–9]. For each of these uses, NPs must be able to travel considerable distances in reservoir rocks. In contrast, the widespread use of nanomaterials causes a significant build-up in the environment with a high risk of contamination [10]. To minimise the threats to the environment and human health, it is crucial to understand these NPs' mobility, sustainability, and ultimate fate.

Surface-active NPs, for instance, can stabilise emulsions and foams for mobility control in improved oil recovery methods [1–6]. These NPs' special features offer a wide range of possible uses in oil reservoirs. To measure specific fluid and/or rock parameters within reservoir formations, functionalized NPs can be introduced as tracers or sensors [7–9]. Some of these applications require long-distance propagation (> 102 m). Retention, which refers to the quantity of NPs retained in porous media during transport, is one important measure to determine NPs transportability in porous media [10]. Retention has two implications in this piece. One involves the injected NPs adhering permanently to stationary surfaces in the reservoir, particularly the rock's grain surface but also the interface between the flowing saline and any remaining oil [10]. The design of slug size and concentration is impacted by this kind of irreversible deposition, particularly in situations where it's crucial to preserve the NPs concentration in the dispersion [11–14]. Reversible NPs adhesion to stationary surfaces is the second. The speed of propagation of the leading and trailing edges of a slug of dispersion is impacted by this form of adsorption (in comparison with the speed of the flowing phase containing the NPs) [15, 16]. These speeds are crucial for evaluating arrival times or remote sensing-derived NPs placements in the reservoir (obtained at production wells).

Experimental studies to evaluate NPs mobility and retention in water-saturated glass-bead/sand packs started in the last ten years [11, 17, 18]. One-wall carbon nanotubes, silica, fullerene, alumoxane, copper oxide, titanium oxide, iron oxide NPs, and other materials have all been tested as nanomaterials. The results of the experiments revealed distinct breakthrough curves for several nanomaterials [19–23]. This suggests that a porous medium's ability to retain a particular type of NP is a quality of both the substance and the medium. This is not a logical conclusion because, for many NPs, van der Waals forces serve as the primary attraction between the grain surface of the porous medium and the NP [16, 24]. Accordingly, the medium's specific surface area should be the main factor influencing the medium's ability to adsorb substances [25]. Laboratory tests have equally been performed for particular nanomaterials to assess the impact of transport conditions on particle retention in porous media. [21] investigated the flow rate effect on the retention of fullerene NPs in water-saturated sand packs. Smaller flow rates kept more NPs in the same column, according to their findings. [26] found that iron NPs effluent history plateau values decreased with flow rate. Solution salinity and pH were discovered to have an impact on titanium NPs retention in column floods [27]. In several of those trials using post-flush, the recovery of NPs was estimated to be a portion of the amount that was injected, ranging from 50 to 99%. Recently, many simulation works have monitored NPs transport through saturated porous media under diverse circumstances [10, 23, 28–30].

Despite the above-mentioned achievements, research on NPs migration in porous media, however, still needs attention, particularly in the following three areas: (i) the impact of ionic strength; (ii) the impact of particle size and concentration; and (iii) mathematical models of NP transport that have been verified by trustworthy experimental data [6, 31, 32]. Regarding the first factor, it is important to further research on how ions, particularly the presence of divalent or monovalent ions, which are common in oil reserves, affect particle transit. The impact of cations on the transport behaviour of NPs has been well evaluated [10, 11, 28]. When compared to the monovalent cation Na^+, it is anticipated that the divalent cations Mg^{2+}, Ca^{2+}, and Ba^{2+} will be more efficient at destabilising NPs and causing greater agglomeration, hence lowering the transit rate [33, 34].

Predicting the subsequent environmental processes of NPs requires knowledge of both their occurrence and toxicity as well as their transit in environmental media. NPs can be carried with the flow in porous medium because they are colloidally suspended [23]. However, co-existing NPs' environmental behaviour and biological efficacy could have an impact on the porous media during transport and retention [23]. Even though some studies have concentrated on the transport of NPs in porous media with various influencing parameters [20, 28, 35], few studies, particularly those that deal with the environmental toxicity, have systematically structured these influencing factors and their interaction mechanisms. In this regard, the application of an environmentally friendly NP in EOR and its transport through saturated porous media is a call for concern.

The use of NPs or materials with nanoscale domains in bio-ceramics, such as the creation of nanoparticle-hydroxyapatite (HAP), has increased the field's relevance for nanotechnology [36]. The development of the calcium phosphate ceramic material known as HAP depends on the combination of the calcium/phosphorus atomic ratio (Ca/P) [37, 38]. In terms of performance and application in various processes, researchers found that HAP performs better than larger-sized hydroxyapatite. Although it varies significantly depending on synthesis techniques and chemical modification, the Ca/P stoichiometric ratio for pure HAP is found to be 1.664 0.005 [37, 38]. HAP is the hydroxyl ion (–OH–) terminal member of the apatite group and has the chemical formula Ca 10 $(PO\ 4)_6(OH)_2$.

HAP stands out due to its outstanding bioactivity, low cost, and biocompatibility. Studies have shown that there is no risk associated with exposure to the Ca/P particle at the dosages commonly used in clinical settings, cosmetics, healthcare services, and biomedicine [39–42], making it safe to be applied in the environment. It has been researched and proven to be helpful in a variety of applications, including tissue engineering, optical applications, bone regeneration, catalysis, and adsorption. HAP includes an OH^- ion, as well as the functional groups PO_4^{3-} and CO_3^{2-}. These HAP features are defined by the alterable Ca–O, C–O, P, and O–P–O bonds that result in fluid adsorption with surfactant ions. HAP has recently demonstrated excellent abilities in enhancing oil recovery mechanisms through IFT reduction and wettability alteration of sandstone. These abilities were observed at varied HAP concentrations, temperature, and brine concentration [45]. It exhibits an equally good ability in oil displacement through sandstone flooding at high ionic strength [48]. Furthermore, HAP equally demonstrates great potential in drilling mud formulations, both in cutting transport and as a fluid loss additive [49].

Our research's main objective is to measure HAP adsorption while it is transported across porous media under a single-phase flow condition at varied ionic strengths. In order to do this, we performed a large number of NPs transport tests using consolidated brine-saturated sandstone core plugs, systematically altering particle characteristics at high temperature in order to mimic the reservoir conditions. Every experiment's breakthrough curve, also known as the NP effluent concentration history, was noted, and the particle adsorption during injection and after a protracted post-flush were both estimated.

This study equally examines the effects of electrolyte solutions with monovalent cations on particle transport behaviour, for both large and small particles, in order to advance our understanding of how NPs move through saturated porous media with different salinities.

2 Materials and Procedures

2.1 Materials

Material	Chemical formula	Molecular weight	CAS number	Supplier
Sodium dodecyl sulphate (SDS)	$NaC_{12}H_{25}SO_4$	288.38 g/mol	151-21-3	Tay Scientific Instruments Sdn. Bhd Malaysia
Calcium 4-nitratre tetrahydrate	$Ca(NO_3)_2 \cdot 4\ H_2O$	236.15 g/mol g/mol	13477-34-4	Tay Scientific Instruments Sdn. Bhd Malaysia
Disodium hydrogen phosphate	Na_2HPO_4	141.959	7558-79-4	Tay Scientific Instruments Sdn. Bhd Malaysia
Sodium hydroxide	NaOH	39.997 g/mol	1310-73-2	VNK SUPPLY & SERVICES Johor Bahru Malaysia
Hydrochloric acid	HCl	36.47 g/mol	7647-01-0	VNK SUPPLY & SERVICES Johor Bahru Malaysia
Sandstone core plugs	XXXX	XXXXX	XXXX	Sarawak Oil Field Malaysia

2.2 Procedures

2.2.1 Synthesis of HAP, Characterisation, and Fluid Preparation

Disodium hydrogen phosphate and calcium nitrate 4-hydrate were used in the wet chemical technique (co-precipitation) to synthesise HAP, which was then in situ surface functionalized with sodium dodecyl sulphate. In order to confirm the presence of HAP and its characteristics, the synthesised NPs were analysed using Fourier transform infrared spectroscopy (FTIR), particle size analysis (PSA), X-ray diffraction (XRD), and zeta potential analysis (ZP), respectively. To evaluate the adsorption of NPs on the rock surface, post-characterisation was done on sandstone cores both before and after flooding with NPs. This involved using x-ray diffraction (XRD), field emission scanning electron microscopy (FESEM), electron scanning microscopy (SEM), and elemental composition (EDX).

Nanofluids (NFs) with concentrations between 0.001 and 0.1 wt% were formulated using brine solutions with a range of 5000–30,000 ppm. The selection of this concentration range was based on the literature (optimal NF concentration [5, 7, 32] for EOR applications). Concentrations beyond 0.1 wt% run the danger of blocking pore channels, triggering rapid aggregation, damaging the formation, and degrading permeability [25, 43]. An RST Brookfield rheometer (Rheo3000, USA), which has an operating temperature range of 25–80 °C, was utilised for measuring the viscosity of the brine. The dried NPs were gathered, weighed, and mixed with brine solution in a beaker. The mixture was then heated to 28 °C and stirred for five minutes using a magnetic stirrer.

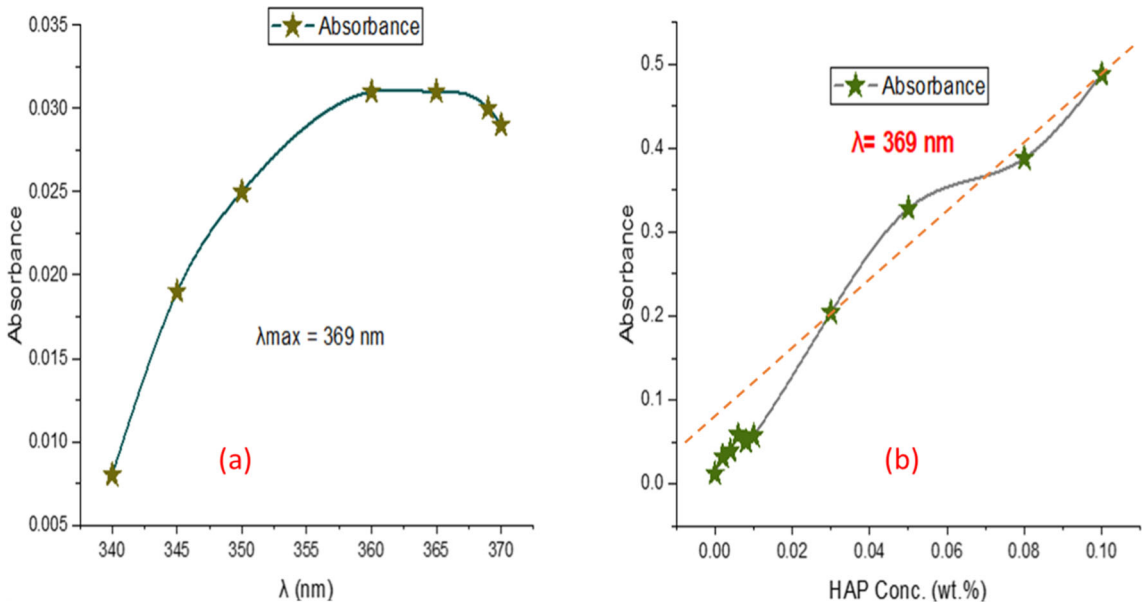

Fig. 1 Absorbance measurements with **a** maximum wavelength determination and **b** molar absorptivity

The generated solution was then homogenised for 15 min in a Branson DHA-1000-E, 100 W, 40 kHz, Danbury, ultrasonic bath to reduce agglomeration.

2.2.2 Absorbance Measurements and Molar Absorptivity Determination

The NPs concentration before and after flooding was determined using HAP's absorbance and molar absorptivity. A UV–VIS spectrometer was used to evaluate the absorbance and wavelength prior to preparing fluids with varying concentrations of HAP. In order to determine the NPs' maximum wavelength, the concentration was first maintained constant while the absorbance was measured at various wavelengths (Fig. 1a). The maximum wavelength was measured to be 369 nm which was then maintained constant for the subsequent tests. To determine the molar absorptivity, the wavelength was maintained constant while the concentration varied (Fig. 1b). The temperature and pressure were both kept at ambient levels for both trials. The measurements were performed by pouring the prepared sample into the cuvette of the apparatus 3/4 full, gently placing inside the measuring chamber after adjusting all the parameters with respect to the current trial, and then conducting the test. Results of absorbance were plotted against concentration (Fig. 1b). Upon generating the gradient of the slope, the molar absorptivity was then calculated using the Beer–Lambert's Law (Eq. 1)

$$A = \boldsymbol{\xi\lambda c} \tag{1}$$

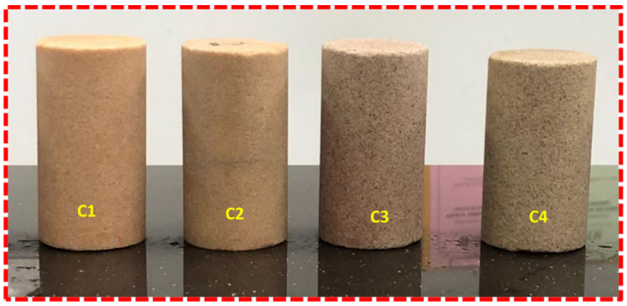

Fig. 2 Sandstone cores for NPs displacement

where A Absorbance, ξ Molar Absorptivity, λ Wavelength and c Fluid Concentration

The molar absorptivity was then used in the same correlation on the measured absorbance to determine the concentration during NP displacement.

2.2.3 Sandstone Cores Preparation

High-permeability sandstone cores (Fig. 2) with the parameters given in Table 1 were used for HAP-NF displacement testing. The four high-permeability sandstone cores are all from the same reservoir and have similar characteristics. The cores were cleaned in a Soxhlet extractor with toluene and acetone to eliminate contaminants. The cores were then dried for 48 h in an oven set to 100 °C. The dry weight of the cores was calculated by mass balancing. At 25 °C and atmospheric pressure, the porosity was ascertained using a TPI-219 porosimeter after the bulk volume had been measured using a calliper. Then, using a VINCI Liquid Permeameter at 25 °C

Table 1 Petrophysical properties of sandstone core samples

Core	Length (cm)	Diameter (cm)	Porosity (%)	Permeability (mD)
C_1	7.1	3.5	25.6	295.031
C_2	7.6	3.6	21.2	283.389
C_3	7.0	3.5	26.5	314.215
C_4	7.4	3.5	27.3	405.103

Where the brine concentration used for each core was C_1(5000 ppm), C_2(10,000 ppm, C_3(20,000 ppm), and C_4(30,000 ppm), respectively

and under atmospheric pressure, the permeabilities of the cores were calculated, and the findings recorded accordingly (Table 1). Prior to the NPs recovery testing, the cores were then completely saturated with brine and compressed at 2000 psi for 24 h. The porosity and permeability measurements were repeated after each test.

2.2.4 Nanoparticles Displacement

Prior to conducting the transport tests, porous medium was characterised, including the estimation of porosity and permeability. The initial transport test was the suspension of HAP in 5000 ppm of brine and passing it through porous sandstone media. After injecting 0.8 PVs, HAP was discovered in the outlet. The amount of NP in the effluent gradually increased before dropping to zero. Then, until the 5th PVs, the NP concentration quotient (C_i/C_O) values varied. The NPs concentration thereafter decreased until it was zero at the sixth PVs. The experiment was repeated at respective concentrations of 10,000 ppm, 20,000 ppm, and 30,000 ppm. To replicate the reservoir environment, all experiments were conducted at a temperature of 80 °C (based on the equipment temperature limitation). For each trial, the HAP concentration was held constant at 0.1 wt%.

The core flooding tests were conducted using high temperature, high pressure (HTHP) equipment from Fars EOR Technologies. Temperature and confining pressure are controlled by an oven and a hydraulic pump, respectively. Different injection configurations are possible with the system thanks to three piston-like accumulators and a core holder. For the purpose of pumping injectants from the accumulator through the core, the apparatus was connected to a Teledyne ISCO pump. The experimental setup is shown schematically in Fig. 3. Before each NPs experiment, the instrument was cleaned, and NFs and brine were added to the accumulators. The oven temperature, the injection fluid flow rate, and the confining pressure were all adjusted to 80 °C, 0.4 mL/min, and 1800psi, respectively. The initial brine solution (5000–30,000 ppm) was displaced and each core was saturated with 2 PV of NPs. After that, brine was once more injected up till the NPs break through. Samples of nanofluids were taken periodically at the effluent to measure the absorbance and the concentration deduced using the Beer–Lambert's Law (Eq. 1).

3 Results and Discussions

3.1 FTIR

The chemical characteristics of powder samples can be ascertained using FTIR. The most distinct functional groups in the FTIR spectrum of the synthesised nano-hydroxyapatite are the phosphate group (PO_4^{3-}) and hydroxyl group (OH) (HAP). The results of the analysed HAP FTIR spectrum are shown in Fig. 4. The stretching modes of the hydroxyl groups in water molecules that have been adsorbed on HAP are linked to the bands at 2849.85 and 2917.84 cm^{-1} [40]. These results showed that the surface of HAP was adsorbed with a considerable quantity of structural OH groups and a minor amount of water molecules from the aqueous solution. When it comes to (P–O) bonds, the band at 1028.56 reflects the symmetric stretching mode, while the bands at 602.04 and 55, 06 represent the asymmetric bending vibrations of (P–O) bonds attributable to PO_4^{-3} [44]

3.2 PSA Analysis

The distribution of HAP was examined using the Malvern Zeta Sizer version 7.11. The findings reveal that the majority of the particles are nanosized, ranging from 220 to 450 nm, with only a small number being micrometre-sized. The particles' average hydrodynamic diameter, which is in the nanometre range and can be recommended for use in EOR, is 328.7 nm (Fig. 5) [45–48]. Due to the pore channels' micrometre-sized size, the NPs' diameters are appropriate for EOR. The growth brought on by the adsorption of water molecules during the fluid preparation process could also be credited with the increase in particle sizes.

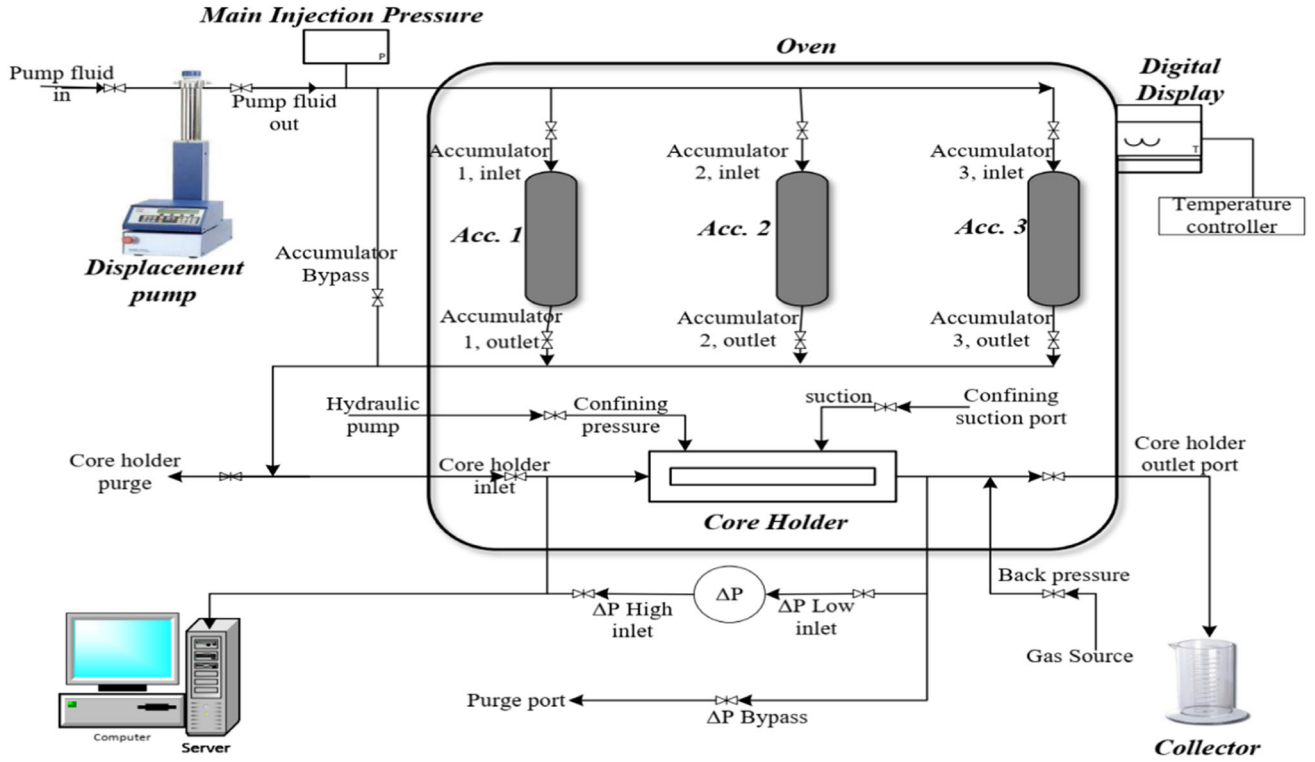

Fig. 3 Fars EOR technology setup for flooding

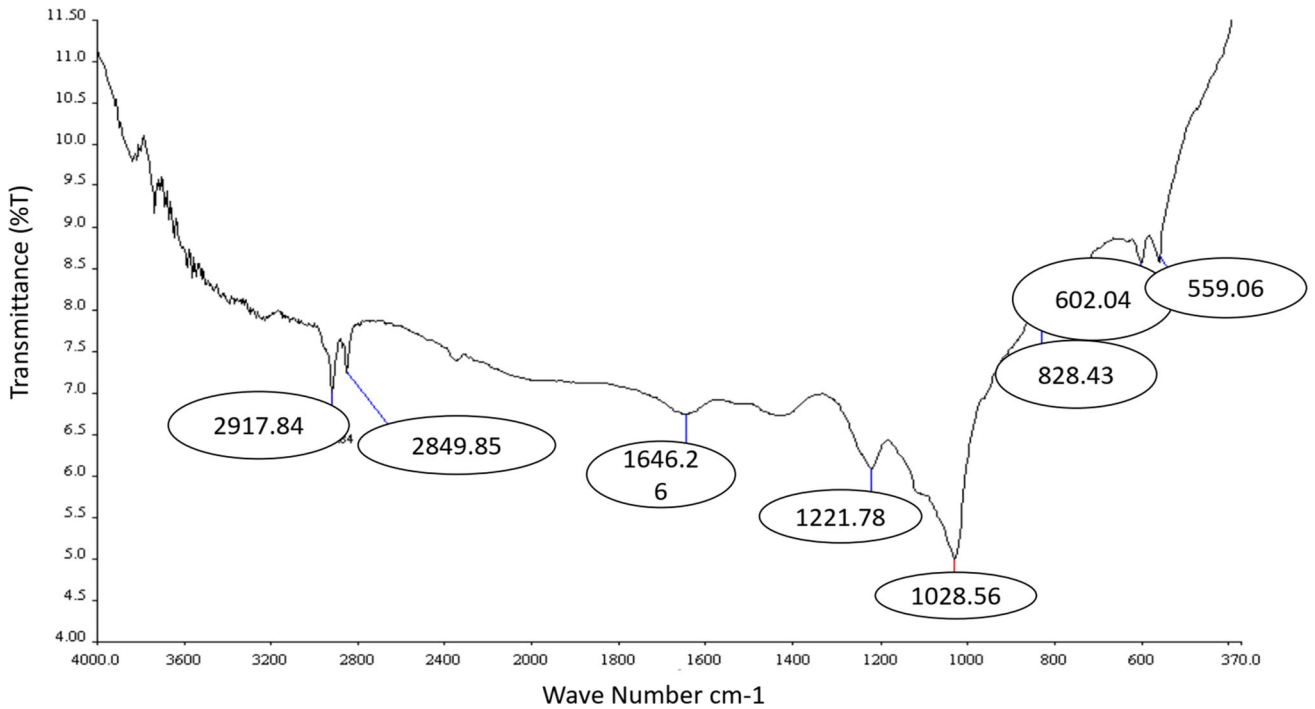

Fig. 4 FTIR spectra

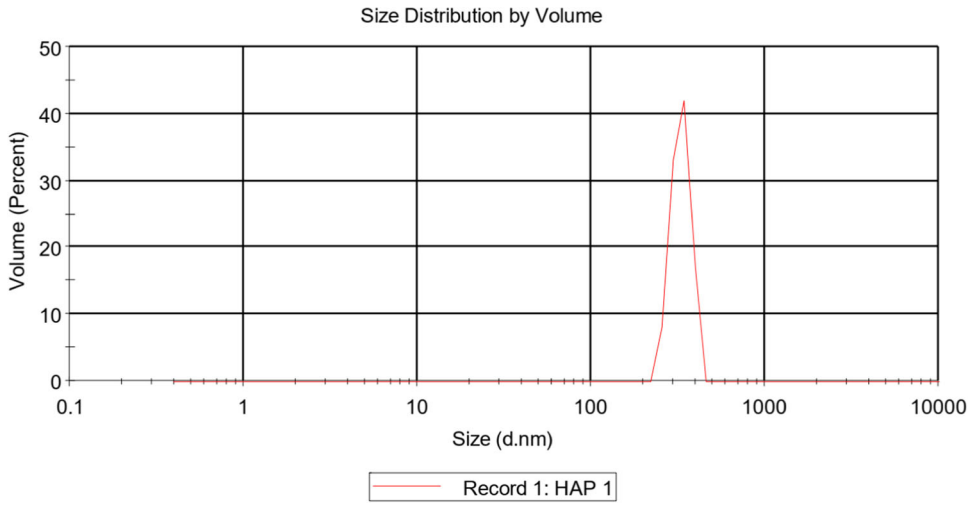

Fig. 5 PSA spectra

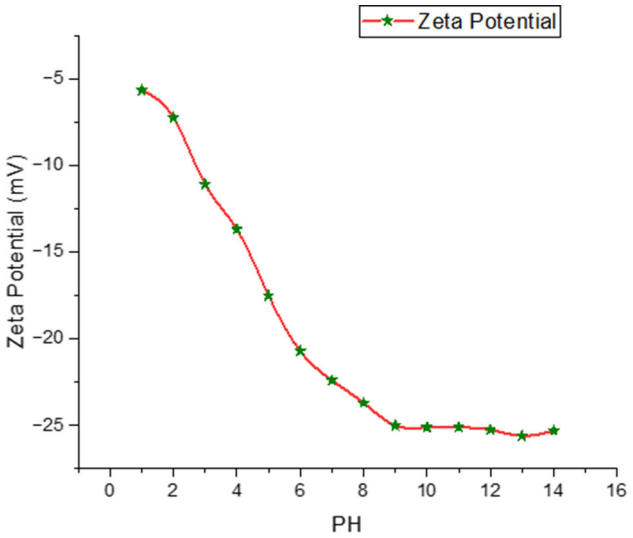

Fig. 6 ZP spectra

3.3 Zeta Potential

The most used stabilisation test for determining if compounded NFs have stable dispersion is sedimentation. But because it takes a lot of time and produces insignificant data, this method is ineffective for assessing HAP dispersion stability. In order to investigate the dispersion stability of the generated NFs, ZP measurements were carried out to quantify the surface charge. ZP as a function of pH was calculated using a Malvern Zeta Sizer version 7.11. The pH range at which the greatest number of hydroxyl ions is dispersed on the surface of the HAP was determined (Fig. 6). The HAP positive charges could be neutralised by the SDS attachment at a pH of 1.69 and replaced with negative SDS ions (acidic). The ZP varies from − 5.69 mV to − 27.2 mV between pH values of 1.69 to 12.8, according to the results, demonstrating that the particles are more stable in a basic medium [45, 49]. Instable suspensions, most likely brought on by agglomeration, are indicated by ZP values of NFs less than 5 (5.0 mV). The average ZP value demonstrates the high stability of the in situ modified HAP. The magnitude suggests if the colloidal system might be stable. A significant negative or positive ZP will cause all of the particles in suspension to reject one another and have no tendency to stick together. HAP can be suggested for EOR applications since it exhibits colloidal stability and dispersion with a ZP of − 27.2 mV, which implies long-term fluid stability [40].

3.4 XRD

In order to investigate the sample's structural details, powder X-ray diffraction was performed. The XRD patterns of the HAP are shown in Fig. 8. The pattern's sharper peaks suggest enhanced crystallinity. There is excellent agreement between the peak positions and the JCPDS (09432) [50, 51]. As can be seen, the hydroxyapatite XRD patterns with the diffraction peaks produced at 2.82, 2.79, and 2.72 as well as the other d-spacing values fully match the hexagonal system with primitive lattice. The results of the XRD analysis used in this analysis agree well with literature. The peaks were solely crystalline in structure and consisted of the hexagonal HAP phase; no other secondary phases, such as calcite, were found (Fig. 7) [52]. The large peaks around peaks (002) and (211) show that the crystallite size was on the order of a nanometre scale [53, 54]. The peaks that represent the (112), (300), and (202) reflections, however, are overlapping as a result of peak broadening [40]. This shows that crystallinity and crystal size may have reduced, and the reduction may have been caused by the presence of di-hydrogen phosphate.

The sandstone outcrops used for the NF displacement were examined before and after flooding using XRD, FESEM, and SEM in order to look into the NF adsorption and retention in the sandstone porous media. Despite

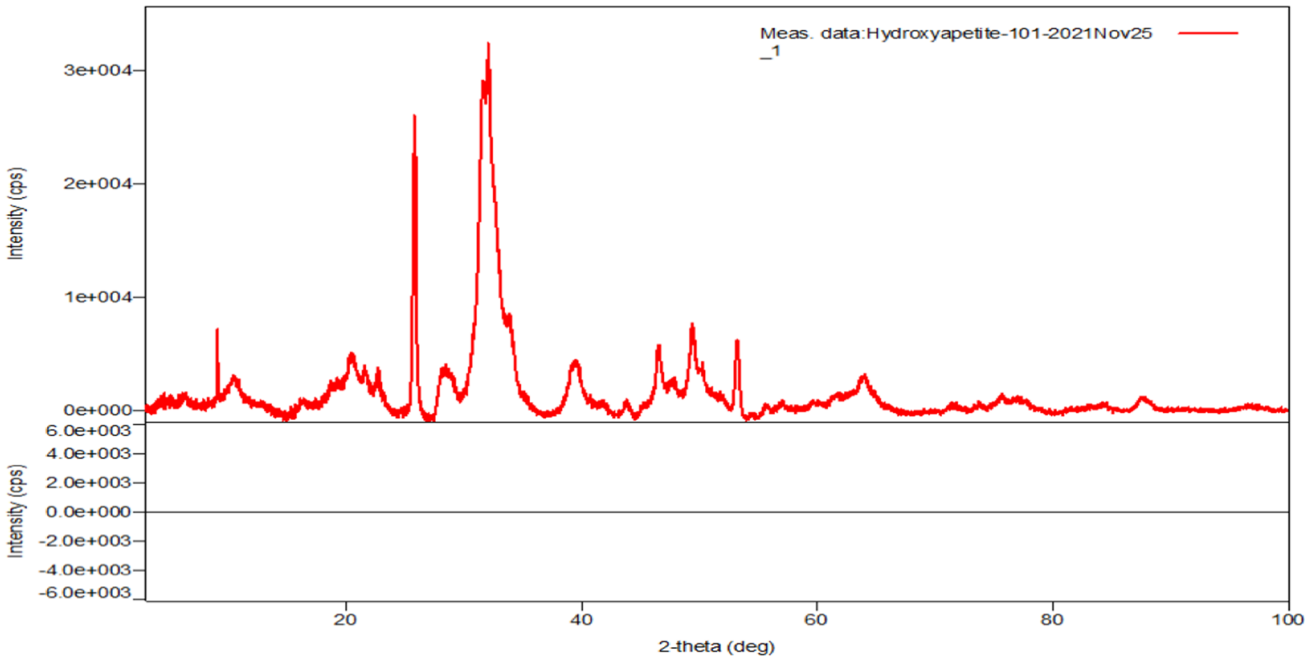

Fig. 7 X-ray diffraction spectra for HAP

quartz being the most common mineral, the XRD data show that feldspar and melanite are both present in almost all of the supplied samples as small components. According to the crystallography (Fig. 8a and b), HAP was discovered on quartz after flooding, proving that it was maintained in the sandstone. HAP altered the pre-NF mineral composition of the sandstone, which initially included quartz (92.2%), melanite (5%), and feldspar (2.8%). Figure 8a consists of quartz, melanite, and feldspar, while Fig. 8b consists of quartz, melanite, feldspar, and HAP. There are like changes in the peak values from 8a to 8b, indicating that the adsorption of HAP slightly modified the mineral content of the rock.

3.5 SEM Analysis

To determine whether the retained NPs are adsorbed onto the rock surface or if they formed clusters with pore channels, SEM pictures of the crushed sandstone were collected both before and after the flooding. As compared to the rock sample before flooding (Fig. 9b), traces of HAP were found deposited on the rock after flooding (Fig. 9d). The findings showed that the majority of the particles were adsorbed on the rocks and that there were few clusters form (Fig. 9c) present. This suggests that, in contrast to traditional NPs, the adsorption of the particles on the rock can cause them to stay in the reservoir for longer periods of time. The adsorption could equally be influenced by the presence of SDS since surfactants have a high ability to absorb on rock surfaces [55–58]. This long-term retention also causes a long-term change in wettability, which is helpful for EOR [16, 32, 59]. The few observed clusters could be attributed to the NF stability as explained by the ZP analysis in Sect. 3.3, resulting from electrostatic repulsion between negatively charged HAP particles.

3.6 FESEM Analysis

Prior to the NPs adsorption, FESEM images were taken at a reduced scale to better understand the mechanism of NPs adsorption on the rocks. Most of the particles were adsorbed with few clusters, confirming the SEM analysis and NF stability (Fig. 10). Due to the size of the particles, the flow of NPs through porous medium displays a Brownian motion [60–62]. Several forces, such as the Van der Walls forces, draw in potential forces and regulate the interaction between the particles and the walls of the porous media [63, 64]. The NPs and the porous medium wall are attracted to and repel each other, causing adsorption and desorption to occur [56, 65]. Diffusion, convection, and hydrodynamics in particular play a significant impact in the flow of particles across porous media [66]. However, born repulsion and hydrodynamic forces influence the adsorption of NPs onto the surface of rocks, respectively. The born repulsion that develops as the surface of the particle and the walls of the porous media come into contact influences the adsorption of NPs onto the surface. When NPs move through porous media, hydrodynamic forces that are low will cause the particles to be suspended onto the pore surface, where they may become adsorbed depending on the surface charge [67]. This is in contrast to how the hydrodynamic force governs the suspension of

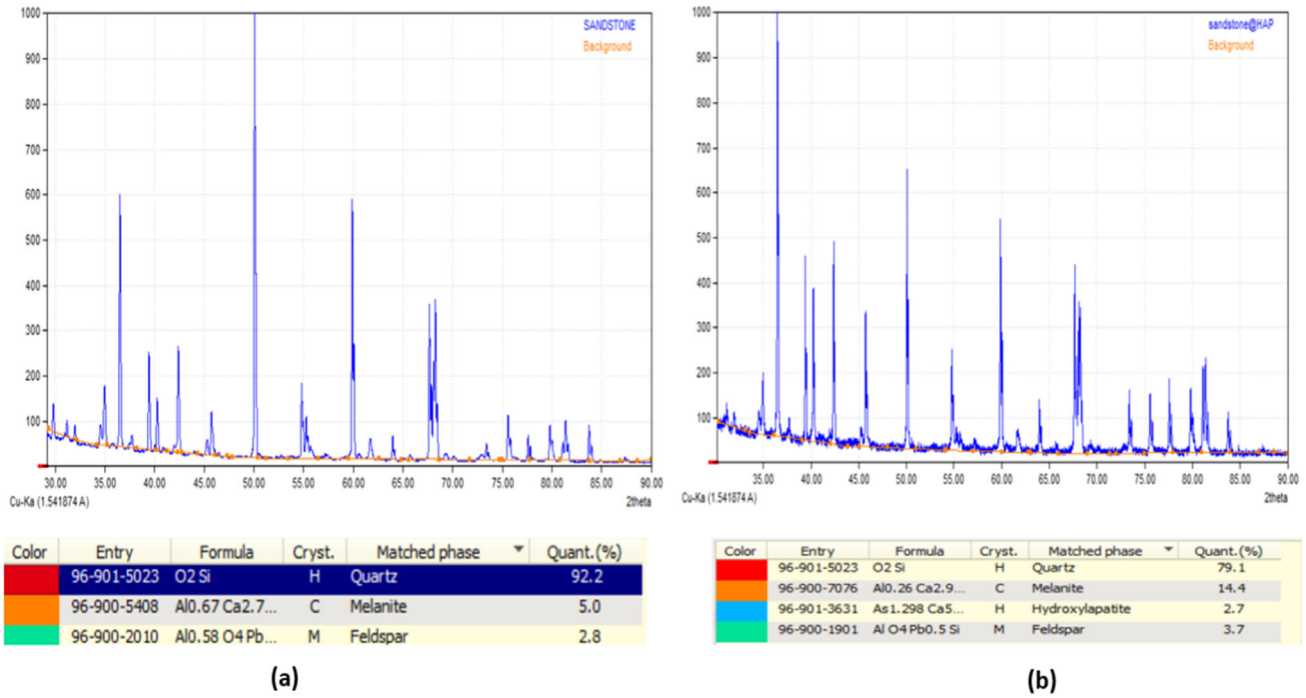

Fig. 8 Post-analysis XRD spectra for **a** sandstone and **b** sandstone with HAP

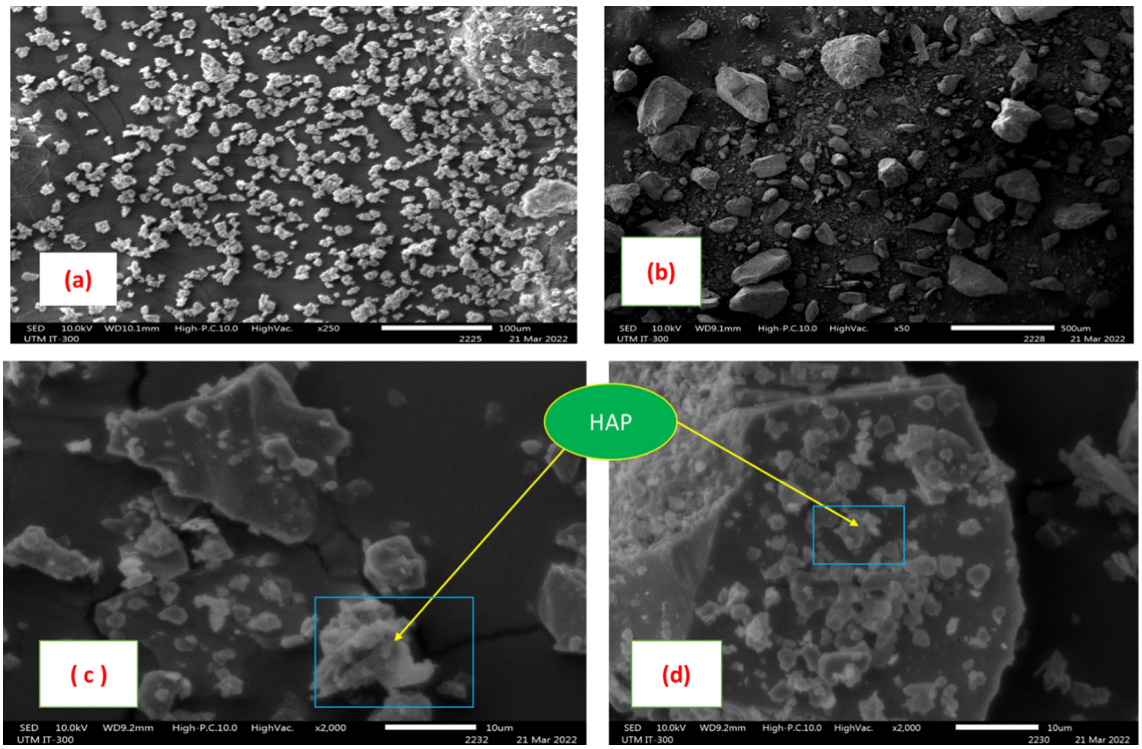

Fig. 9 SEM spectra with **a** HAP, **b** sandstone, **c** and **d** sandstone with NPs adsorbed

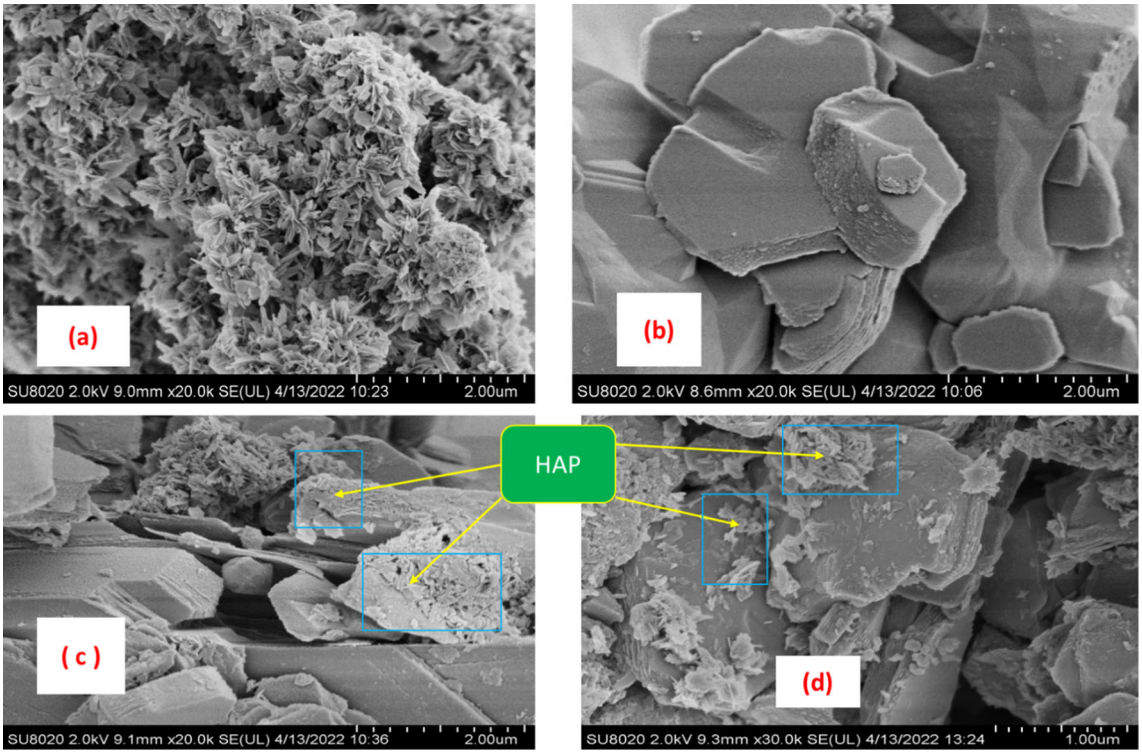

Fig. 10 FESEM spectra with **a** HAP, **b** sandstone, **c** and **d** sandstone with NPs adsorbed

a flowing liquid and is dependent on the surface charge of the NPs. As a result, the high adsorption of HAP onto the sandstone rock as indicated in Fig. 10d concludes that born repulsion was dominant.

3.7 EDX Analysis

According to the EDX study, the presence of calcium and phosphorus with high percentages in (Fig. 11a) is a result of HAP, but the high concentrations of silicon and oxygen in (Fig. 11b) are attributed silicon dioxide (quartz), the dominant element in sandstone as initially confirmed by the XRD results. Traces of other elements in small amounts could be attributed to felspar and melanite. The presence of HAP is confirmed with the inclusion of two previously non-existent elements (calcium and phosphorus) in (Fig. 11d), with a reduction in the fractions of silicon and oxygen as compared to (Fig. 11b). The calculated Ca/P molar ratio, which was obtained from the elemental composition, came out to be 1.69, which is less than 2 and falls within the permitted range of HAP values. Calcium and phosphorus should have a standard HAP ratio of 1.67 [40].

3.8 Brine Viscosity

The ionic solution's viscosity is influenced by three factors: Brownian motion, Debye–Hückel interaction (electrostatic potential caused by all surrounding ions), and structural temperature impact (the tightening or loosening of the structure caused by hydrated or un-hydrated ions, respectively) [26, 61]. The Debye–Hückel interaction and Brownian motion always contribute favourably to the viscosity of any brine [68]. However, the influence of structural temperature on the viscosity of brine varies depending on the type of salts, either positively or negatively [69, 70]. Three mechanisms can be used to treat the physical cause of viscosity. First, each ion is represented as a separate particle that, through Brownian motion, transfers momentum from one region of the liquid to another. Second, the Debye–Hückel theory, which states that "a particular resistance to shear directly correlates with viscosity and accounts for the influence of the ionic interaction". Thus, the Brownian motion and Debye–Hückel interaction always make positive contributions to the viscosity of any ionic solution. Finally, the presence of ions changes the structure of water, affecting how strong the connections are. Depending on the kind of salts used, this final factor affects the ionic solution's viscosity either favourably or unfavourably [68]. Due to the presence of NaCl, the electrostatic attraction between the water layers in this case is heightened, resulting in an increased viscosity of the brine. The overall cathodic current for both dilute and concentrated NaCl electrolytes increases with increase in temperature (Fig. 12). For NaCl electrolytes (5000–30,000 ppm), an

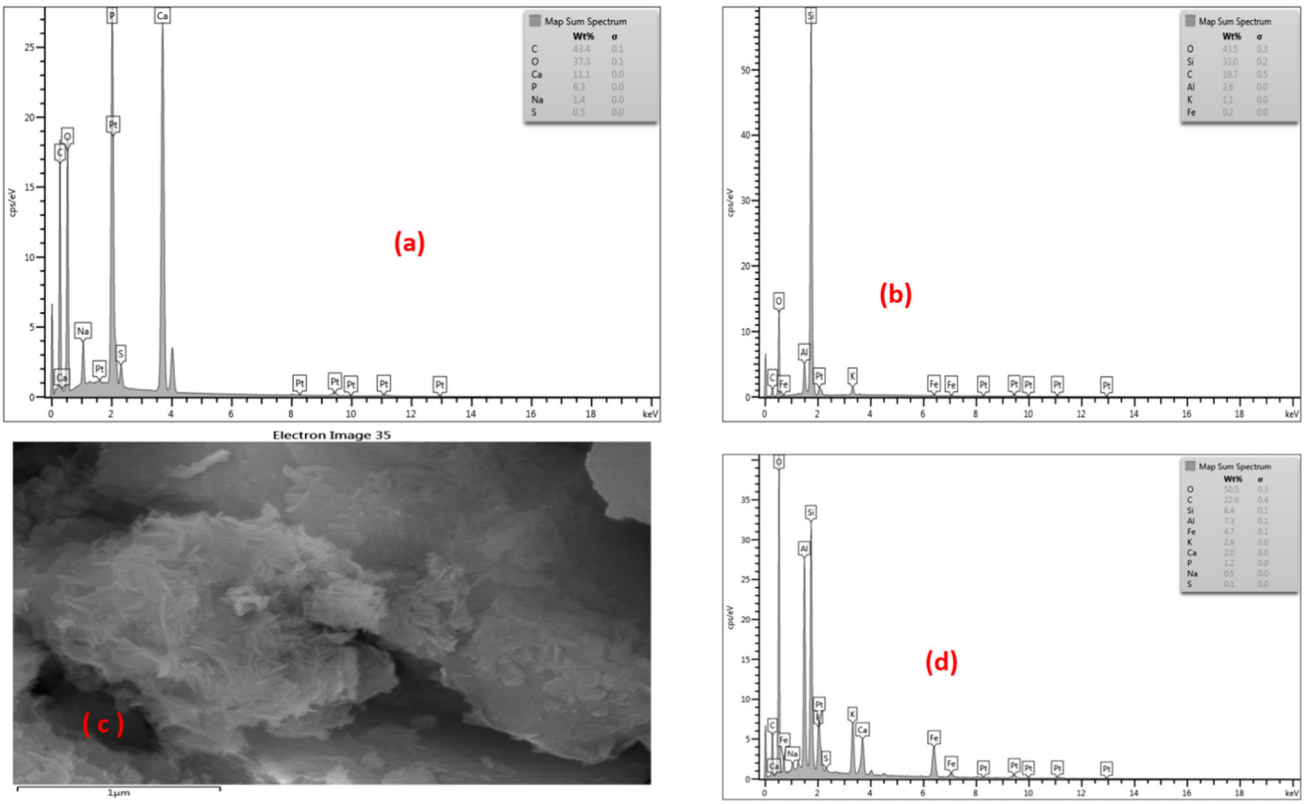

Fig. 11 EDX spectra with spectra with **a** HAP, **b** sandstone, **c** image spectrum and **d** sandstone with NPs adsorbed

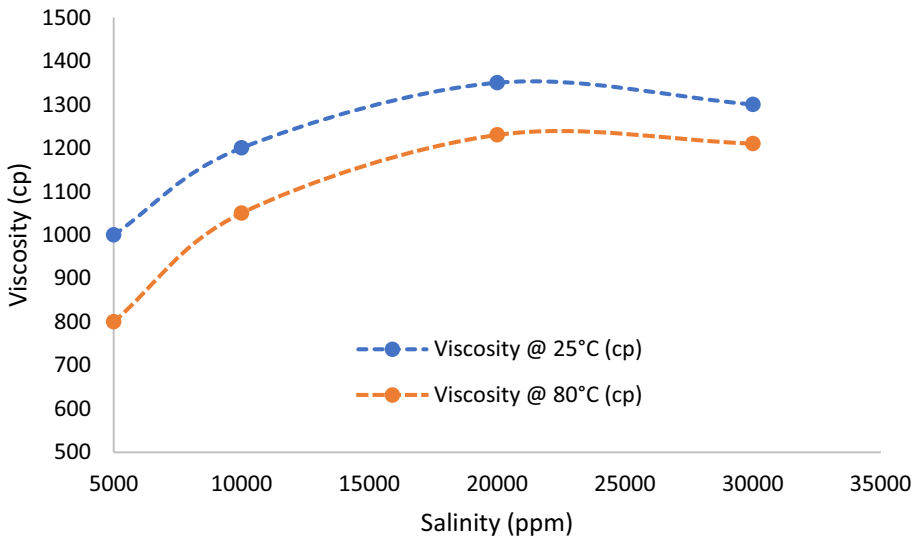

Fig. 12 Brine viscosity at varied temperatures

increase in temperature leads to higher conductivity, lower viscosity, and oxygen concentration [71].

3.9 Nanoparticles Displacement

The findings from the NPs transport across porous media are presented in Table 2. Figures 13 and 14 display breakthrough curves for NP transport studies through porous sandstone media. The two main methods for retaining HAP on the sandstone grains are deposition and adsorption, respectively. Therefore, the FESEM, XRD, SEM, and EDX studies demonstrated the presence of HAP on the surfaces of the sandstone grains with (a) 5000 ppm brine, (b) 10,000 ppm, (c) 20,000 ppm, and (d) 30,000 ppm, respectively. According to the findings, a rise in salinity from 5000 to 30,000 ppm led

Table 2 Parameters for transport of NPs through sandstone at different ionic strengths

Brine concentration	5000 ppm	10,000 ppm	20,000 ppm	30,000 ppm
Area	0.00779	0.00684	0.00561	0.00229
PV_{BT}	1.2	1.1	1.3	1.0
R_{NP}	0.65	0.62	0.43	0.23
C_i/C_{omax}	0.001639	0.001826	0.002372	0.000593
Porosity (%)	21.3	19.6	21.5	23.3
Permeability (mD)	275.001	243.369	274.697	395.103
N_0. of PV	5.6	5.6	5.6	5.6

Where each brine concentration used for each core was C_1(5000 ppm), C_2(10,000 ppm, C_3(20,000 ppm), and C_4(30,000 ppm), respectively

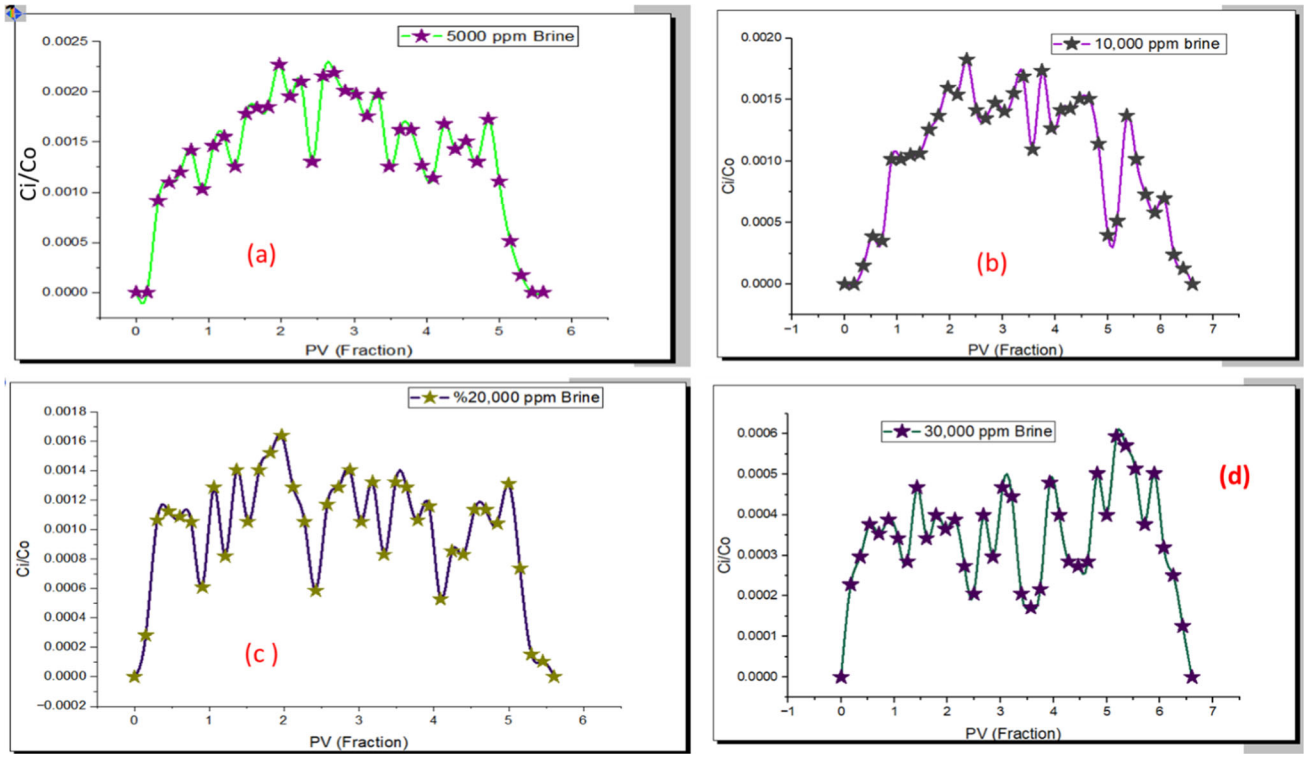

Fig. 13 Nanoparticles recovery for **a** 5000 ppm brine, **b** 10,000 ppm brine, **c** 20,000 ppm brine, and **d** 30,000 ppm brine

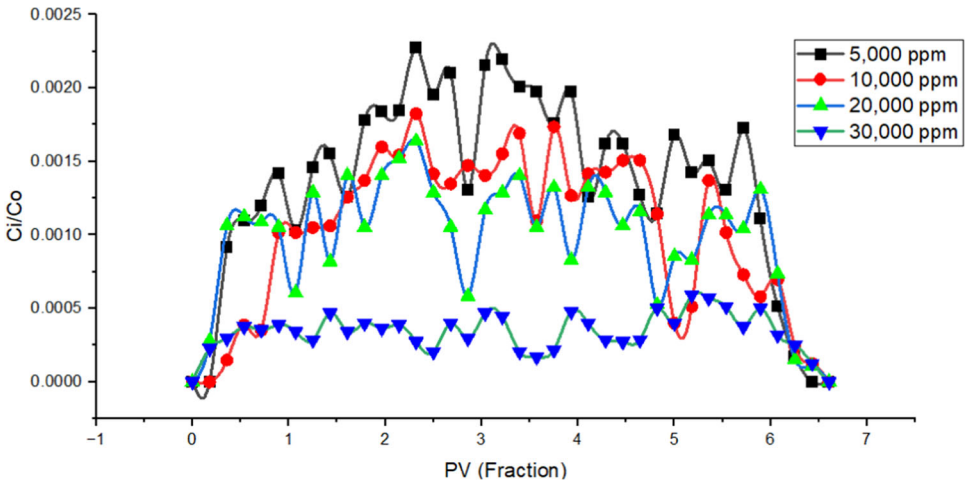

Fig. 14 Cumulative nanoparticles recovery for all the brine concentrations

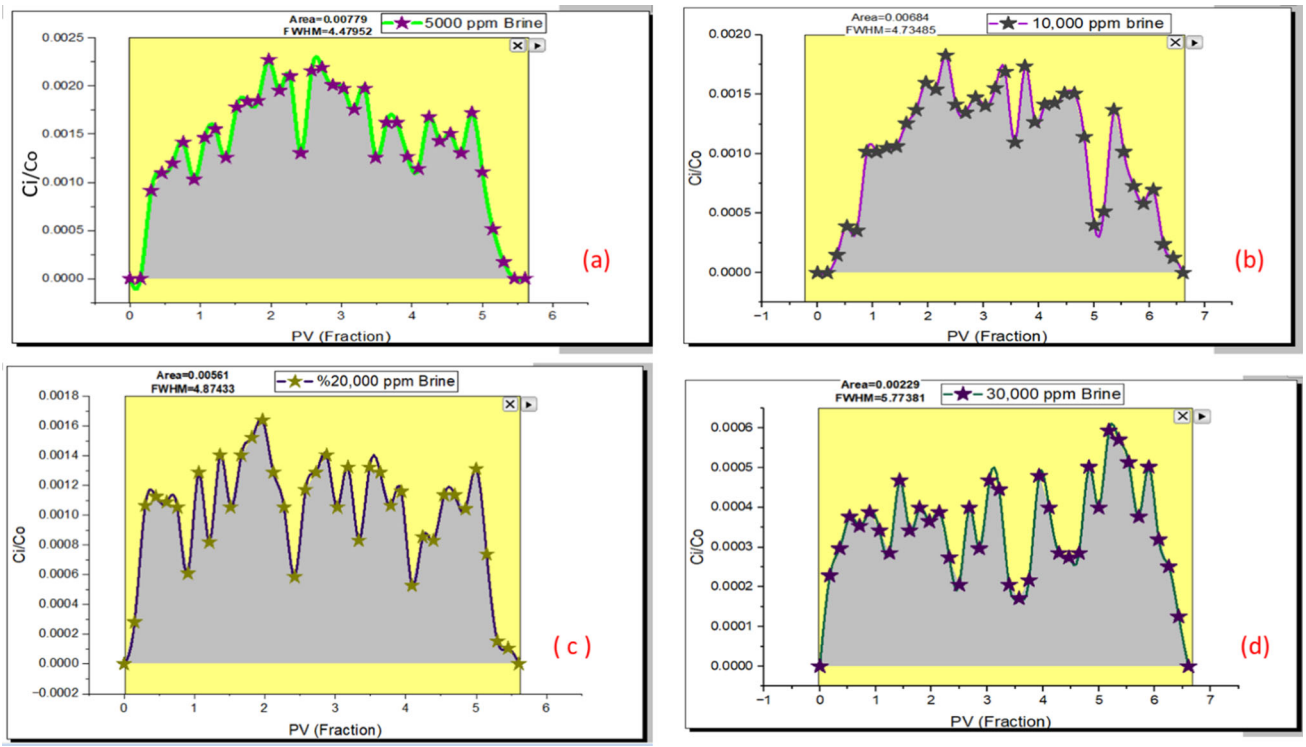

Fig. 15 Area calculations for breakthrough curves corresponding to **a** 5000 ppm brine, **b** 10,000 ppm brine, **c** 20,000 ppm brine and **d** 30,000 ppm brine

to a decline in HAP recoveries from 0.65 to 0.23%, respectively. In addition, it was found that the salinity rise resulted in an extension of the NP's breakthrough time and experiment duration. Another factor that was noted during the tests was a decrease in the outlet's maximum NP concentrations (C_i/C_O max). The NP percentage recovery was calculated by measuring the area under the breakthrough curves (Fig. 15) and applying it in Eq. (2)

$$\text{NP \% Recovery} = \frac{\text{Surface area under BT}}{\text{No. of PVs in suspension}} \times 100 \qquad (2)$$

Two processes are related to how long NPs stay in the reservoir. Adsorption on the rock is favourable for EOR, whereas pore channel obstruction is detrimental to EOR [6, 72]. The permeability measurements conducted before and after the NPs flooding through core plugs, however, showed that there was negligible pore channel obstruction. In light of this, adsorption was the primary cause of the low NPs recovery. Even though numerous studies have reported that, 90% or more of the NPs are retrieved after injection [35, 73–75], complete NPs recovery, on the other hand, results from low adsorption, whereas NPs adhering to rock surfaces and their retention in the reservoir cause long-term wettability changes which is intend beneficial for EOR [31, 76]. Low NPs recovery during EOR also results in low separation costs after oil/NPs production [77]. This result therefore suggests that HAP-NF is a good candidate for EOR processes [7] based on the adsorption affinity onto sandstone Figs. 10 and 11, which will lead to long-term wettability alteration [40, 76] during EOR mechanisms.

The decrease in NP recovery with increased salinity could equally be linked to the agglomeration and aggregation of the NPs at higher ionic strengths, resulting in poor NP mobility through porous media [7, 20, 77–79]. The recovery could also be linked to changes in the porosity and permeability of the cores. There are many different processes that modify the porosity and permeability of a porous medium. These processes include changes in mechanical stress, sedimentation, filtration, and mineral precipitation or dissolution [26, 80, 81]. The change in effective porosity contributing to flow depends on the process that alters the individual pore space [82]. The observed reduction in porosity and permeability is therefore the result of NPs retention.

Due to the presence of clay minerals, sandstones have a tendency to expand at elevated relative humidity, which can have an impact on the material's mechanical characteristics and pore scale impact [83]. Nonetheless, an increased in NaCl concentrations will result in a thinner diffuse double layer (DDL), which will then result in a weaker repulsive force between clay particles. As a result, the specimen clay will tend to show decreased residual swelling pressure

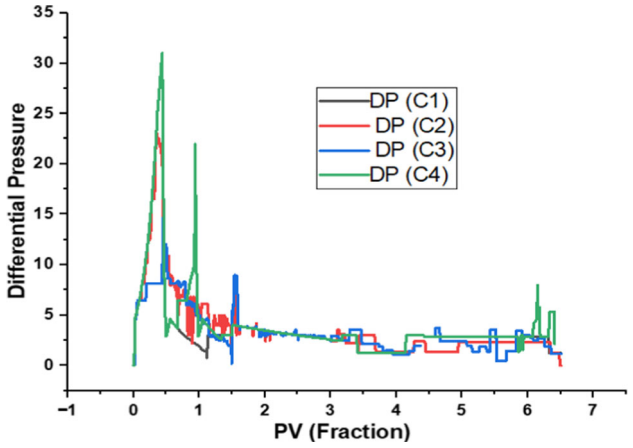

Fig. 16 Differential pressure

with increase in NaCl concentration [84]. Furthermore, clay aggregates increase due to the adsorption of NaCl ions (from brine), which also promote mineral breakdown, increasing permeability as a result [85, 86].

The Fars EOR Technology pressure gauge continuously measured the differential pressure during the flooding experiments. For each of the individual core plugs C_1, C_2, C_3, and C_4, Fig. 16 shows the differential pressure and recovery data. The cores received brine injections up until HAP-NF production ceased. A rise in differential pressure was seen during the first 0.5 PV of brine inundation. The differential pressure fluctuated during the flooding, but it mysteriously increased when brine was introduced at a pressure of about 0.5 PV into this core plug. Some NPs may adsorb, clog pore channels, and reduce the permeability of core plugs as a result. Given that they all came from the same oil field, the differential pressure of the individual core plugs displayed a similar pattern. The tiny discrepancy in permeabilities between them might be the cause of the fluctuation. Absolute permeability increases with salinity, despite numerous studies showing that low salinity floods increase NPs recovery.

4 Limitations and Recommendation

This research was restricted to sandstone cores at high salinities and temperatures. As a result, research into alternate reservoir rock types, like carbonates, is necessary. Additionally, HAP must be checked for floods caused by low salinity. While HAP in this study was produced and functionalized in situ using SDS, other well-known chemicals for functionalizing NPs, such as cationic surfactants and amines, might be studied. The brine chosen for this study was sodium chloride only (monovalent cations in solution). The interaction of HAP with divalent cations can equally be verified. Last but not least, it is strongly recommended to use particle retention models that take salinity and travel duration into account for a detailed understanding of HAP transport through porous media. Additionally, this work was aimed at addressing the effects of monovalent cations on HAP transport and adsorption through porous media. However, NaCl is just one of the many brines found in the reservoir. The application of other cations especially divalent ions on HAP adsorption is thus recommended.

5 Summary and Conclusion

In this study, the NP adsorption of HAP functionalized in situ with SDS while it is transported across porous media under a single-phase flow condition was comprehensively examined. The following conclusions were drawn from the study's findings:

1. The P–O and O–H functional groups seen in the FTIR results showed the formation of HAP, while the crystal lattice of the XRD results suggested the formation of conventional HAP. Furthermore, the ZP data demonstrated the HAP stability in fluids and high temperature settings.
2. An increase in ionic strength causes NP retention to rise, leading to a reduction in NP recovery. This is related to the fact that NPs have limited mobility through porous media when they aggregate and agglomerate at greater ionic strengths.
3. There are two factors linked to the low NP recovery (adsorption on the rock surfaces or aggregation of NPs with the formation of clusters). However, the results of the permeability tests performed on the core plugs before and after flooding, as well as the SEM and FESEM images of the sandstone taken, showed that it is almost certainly due to adsorption.
4. The percentage of recovered NPs after flooding was rather low in comparison with published works. This is because the majority of studies concentrate on NPs that pass through the reservoir without being retained. Two benefits of the low recovery of the NPs with minimal pore obstruction, however, mostly go unnoticed by most people. Due to wettability alteration, long-term adsorption of NPs on the rocks will result in negligible adsorption of oil. Secondly, there will be fewer NPs produced alongside the oil, resulting in lower separation costs after oil production.
5. The majority of research on the transport of NPs across saturated porous media uses simulation. However, in order to comprehend the process at the laboratory scale as well as in the field, equal emphasis needs to be paid to laboratory methods.

Acknowledgements The authors would like to acknowledge the financial support from the Ministry of Education, Malaysia, under the Fundamental Research Grant Scheme (FRGS) via reference number FRGS/PV/2022/03075 and Universiti Teknologi Malaysia for the funding under UTM Fundamental Research (UTMFR) (FRGS/PV/2022/03075; Q.J130000.21A2.06E09; Q.J130000.21A2.06E09). The author's profound appreciation also goes to the unidentified reviewers for their timely and invaluable recommendations. Engr. Dr. Jeffrey Onuoma Oseh is a researcher at UTM under the postdoctoral fellowship scheme for the project "Evaluation of Modified Hydroxyapatite Nanoparticles for Rheological and Filtration Properties Modification in Field-Applicable Drilling Muds". Centre for Teaching and Learning, Universiti Teknologi Malaysia, (R.J130000.7851.5F030, Q.J1300003551.06G68).

References

1. Zhu, G., Liu, Y., Sweeney, S., Chen, S.: Functionalization and grafting of nanoparticle surfaces, vol. 1, no. C. Elsevier, (2018). Doi: https://doi.org/10.1016/B978-0-12-409547-2.13152-X.
2. Zhu, T.; Ogbe, D.O.; Khataniar, S.: Improving the foam performance for mobility control and improved sweep efficiency in gas flooding. Ind. Eng. Chem. Res. **43**(15), 4413–4421 (2004). https://doi.org/10.1021/ie034021o
3. Yakasai, F.; Zaidi Jaafar, M.; Akhmal Sidek, M.; Bandyopadhyay, S.; Agi, A.; Ngouangna, E.N.: Co-precipitation and grafting of (3-Aminopropyl) triethoxysilane on ferro nanoparticles to enhance oil recovery mechanisms at reservoir conditions. J. Mol. Liquids **371**, 121007 (2022). https://doi.org/10.1016/J.MOLLIQ.2022.121007
4. Mamah, S.C., et al.: Bio-polymer modified nanoclay embedded forward osmosis membranes with enhanced desalination performance. J. Appl. Polym. Sci. **139**(27), e52473 (2022). https://doi.org/10.1002/app.52473
5. Agi, A., et al.: Comparing natural and synthetic polymeric nanofluids in a mid-permeability sandstone reservoir condition. J. Mol. Liquids **317**, 113947 (2020). https://doi.org/10.1016/j.molliq.2020.113947
6. Yakasai, F.; Jaafar, M.Z.; Bandyopadhyay, S.; Agi, A.: Current developments and future outlook in nanofluid flooding: a comprehensive review of various parameters influencing oil recovery mechanisms. J. Ind. Eng. Chem. **93**, 138–162 (2021). https://doi.org/10.1016/j.jiec.2020.10.017
7. Ngouangna, E.N.; Zaidi Jaafar, M.; Norddin, M.N.A.M.; Agi, A.; Oseh, J.O.; Mamah, S.: Surface modification of nanoparticles to improve oil recovery mechanisms: a critical review of the methods, influencing parameters, advances and prospects. J. Mol. Liquids **360**, 119502 (2022). https://doi.org/10.1016/j.molliq.2022.119502
8. Chen, P.; Lo Re, G.; Berglund, L.A.; Wohlert, J.: Surface modification effects on nanocellulose-molecular dynamics simulations using umbrella sampling and computational alchemy. J. Mater. Chem. A **8**(44), 23617–23627 (2020). https://doi.org/10.1039/d0ta09105g
9. Vandenabeele, C.R.; Lucas, S.: Technological challenges and progress in nanomaterials plasma surface modification—A review. Mater. Sci. Eng. R: Rep. **139**(November 2019), 100521 (2020). https://doi.org/10.1016/j.mser.2019.100521
10. Singh, H.; Javadpour, F.: Retention of nanoparticles: from laboratory cores to outcrop scale. Geofluids (2017). https://doi.org/10.1155/2017/8730749
11. Wang, C., et al.: Retention and transport of silica nanoparticles in saturated porous media: effect of concentration and particle size. Environ. Sci. Technol. **46**(13), 7151–7158 (2012). https://doi.org/10.1021/es300314n
12. Peng, B., et al.: A review of nanomaterials for nanofluid enhanced oil recovery. RSC Adv. **7**(51), 32246–32254 (2017). https://doi.org/10.1039/c7ra05592g
13. Ngouangna, E., et al.: SPE-217124-MS effect of temperature and particle exposure on hydroxyapatite nanoparticles on wettability alteration of oil-wet sandstone. In: SPE Nigeria Annual International Conference and Exhibition. OnePetro. (2023). Doi: https://doi.org/10.2118/217124-MS.
14. Ngouangna, E., et al.: SPE-217122-MS the effect of low salinity flooding of silica nanoparticles functionalized with (3 Aminopropyl) triethoxysilane on enhanced oil recovery. In: SPE Nigeria Annual International Conference and Exhibition. OnePetrono. Cmc, pp. 1–13, (2023). Doi: https://doi.org/10.2118/217122-MS.
15. Irfan, S.A.; Shafie, A.; Yahya, N.; Zainuddin, N.: Mathematical modeling and simulation of nanoparticle-assisted enhanced oil recovery—A review. Energies **12**(8), 1–19 (2019). https://doi.org/10.3390/en12081575
16. Arain, Z.U.A., et al.: Reversible and irreversible adsorption of bare and hybrid silica nanoparticles onto carbonate surface at reservoir condition. Petroleum **6**(3), 277–285 (2020). https://doi.org/10.1016/j.petlm.2019.09.001
17. Hu, Z.; Zhao, J.; Gao, H.; Nourafkan, E.; Wen, D.: Transport and deposition of carbon nanoparticles in saturated porous media. Energies **10**(8), 1–17 (2017). https://doi.org/10.3390/en10081151
18. Wang, Y.; Li, Y.; Fortner, J.D.; Hughes, J.B.; Abriola, L.M.; Pennell, K.D.: Transport and retention of nanoscale C_{60} aggregates in water-saturated porous media. Environ. Sci. Technol. **42**(10), 3588–3594 (2008). https://doi.org/10.1021/es800128m
19. Taghavi, S.M., et al.: Effects of nanoparticles on the environment and outdoor workplaces. Electr. Physician **5**(4), 706–712 (2013). https://doi.org/10.14661/2013.706-712
20. Kim, I.; Taghavy, A.; DiCarlo, D.; Huh, C.: Aggregation of silica nanoparticles and its impact on particle mobility under high-salinity conditions. J. Pet. Sci. Eng. **133**, 376–383 (2015). https://doi.org/10.1016/j.petrol.2015.06.019
21. Lecoanet, H.F.; Bottero, J.Y.; Wiesner, M.R.: Laboratory assessment of the mobility of nanomaterials in porous media. Environ. Sci. Technol. **38**(19), 5164–5169 (2004). https://doi.org/10.1021/es0352303
22. Kanel, S.R.; Nepal, D.; Manning, B.; Choi, H.: Transport of surface-modified iron nanoparticle in porous media and application to arsenic(III) remediation. J. Nanopart. Res. **9**(5), 725–735 (2007). https://doi.org/10.1007/s11051-007-9225-7
23. Ling, X.; Yan, Z.; Liu, Y.; Lu, G.: Transport of nanoparticles in porous media and its effects on the co-existing pollutants. Environ. Pollut. **283**, 117098 (2021). https://doi.org/10.1016/j.envpol.2021.117098
24. Israelachvili, J.N.: Van der Waals forces between particles and surfaces. Intermol. Surf. Forces (2011). https://doi.org/10.1016/b978-0-12-375182-9.10013-2
25. Zhang, T., et al.: Investigation of nanoparticle adsorption during transport in porous media. In: Proceedings-SPE Annual Technical Conference and Exhibition, vol. 4, no. January 2014, pp. 3161–3180. (2013). Doi: https://doi.org/10.2118/166346-ms.
26. He, F.; Zhang, M.; Qian, T.; Zhao, D.: Transport of carboxymethyl cellulose stabilized iron nanoparticles in porous media: column experiments and modeling. J. Colloid Interface Sci. **334**(1), 96–102 (2009). https://doi.org/10.1016/j.jcis.2009.02.058
27. Choy, C.C.; Wazne, M.; Meng, X.: Application of an empirical transport model to simulate retention of nanocrystalline titanium dioxide in sand columns. Chemosphere **71**(9), 1794–1801 (2008). https://doi.org/10.1016/j.chemosphere.2007.12.030
28. Li, C.; Li, Y.; Pu, H.: 'Molecular simulation study of interfacial tension reduction and oil detachment in nanochannels by surface-modified silica nanoparticles. Fuel **292**(February), 120318 (2021). https://doi.org/10.1016/j.fuel.2021.120318

29. El-amin, M.F.; Alwated, B.; Hoteit, H.A.: Machine learning prediction of nanoparticle transport with two-phase flow in porous media. Energies **16**(2), 678 (2023)
30. Abiz, M.R.; Apourvari, S.N.; Jafari, S.; Schaffie, M.: A simulation study of nanoparticle transport in porous media: effects of salinity and reservoir parameters. Iran. J. Oil Gas Sci. Technol. **10**(2), 90–106 (2021)
31. Yakasai, F.; Zaidi Jaafar, M.; Akhmal Sidek, M.; Bandyopadhyay, S.; Agi, A.; Ngouangna, E.N.: Co-precipitation and grafting of (3-Aminopropyl) triethoxysilane on Ferro nanoparticles to enhance oil recovery mechanisms at reservoir conditions. J. Mol. Liquids **371**, 121007 (2023). https://doi.org/10.1016/j.molliq.2022.121007
32. Yakasai, F.; Jaafar, M.Z.; Bandyopadhyay, S.; Agi, A.; Sidek, M.A.: Application of iron oxide nanoparticles in oil recovery—A critical review of the properties, formulation, recent advances and prospects. J. Pet. Sci. Eng. **208**, 109438 (2022). https://doi.org/10.1016/j.petrol.2021.109438
33. Al, H.N.; Ali, S.; Ralph, K.A.; Patrick, F.: Sequential injection mode of high-salinity/low-salinity water in sandstone reservoirs: oil recovery and surface reactivity tests. J. Pet. Explor. Prod. Technol. **9**(1), 261–270 (2019). https://doi.org/10.1007/s13202-018-0466-z
34. Smits, J., et al.: Synergistic and competitive adsorption of hydrophilic nanoparticles and oil-soluble surfactants at the oil-water interface. Langmuir **37**(18), 5659–5672 (2021). https://doi.org/10.1021/acs.langmuir.1c00559
35. Tian, Y.; Gao, B.; Silvera-Batista, C.; Ziegler, K.J.: Transport of engineered nanoparticles in saturated porous media. J. Nanopart. Res. **12**(7), 2371–2380 (2010). https://doi.org/10.1007/s11051-010-9912-7
36. Padmanabhan, V.P.; Kulandaivelu, R.; Panneer, D.S.; Vivekanan-than, S.; Sagadevan, S.; Lett, J.A.: Microwave synthesis of hydroxyapatite encumbered with ascorbic acid microwave synthesis of hydroxyapatite encumbered with ascorbic acid intended for drug leaching studies. Mater. Res. Innov. **00**(00), 1–8 (2019). https://doi.org/10.1080/14328917.2019.1624940
37. Pham, T.T.T., et al.: Impact of physical and chemical parameters on the hydroxyapatite nanopowder synthesized by chemical precipitation method. Adv. Nat. Sci.: Nanosci. Nanotechnol. **4**(3), 035014 (2013). https://doi.org/10.1088/2043-6262/4/3/035014
38. Ajduković, Z.R., et al.: In vitro evaluation of nanoscale hydroxyapatite-based bone reconstructive materials with antimicrobial properties. J. Nanosci. Nanotechnol. **16**(2), 1420–1428 (2016). https://doi.org/10.1166/jnn.2016.10699
39. Jagadale, P.N.; Jagtap, P.P.; Joshi, M.G.; Bamane, S.R.: A prototype synthesis and characterization of hydroxyapatite bioceramics nanocrystallites. Adv. Mater. Lett. **7**(4), 325–329 (2016). https://doi.org/10.5185/amlett.2016.5837
40. Ngouangna, E.N., et al.: The effect of hydroxyapatite nanoparticles on wettability and brine-oil interfacial tension as enhance oil recovery mechanisms. J. Pet. Sci. Eng. **218**, 110941 (2022). https://doi.org/10.1016/j.petrol.2022.110941
41. Mishra, V.K.; Rai, S.B.; Asthana, B.P.; Parkash, O.; Kumar, D.: Effect of annealing on nanoparticles of hydroxyapatite synthesized via microwave irradiation: structural and spectroscopic studies. Ceram. Int. **40**(7 Part B), 11319–11328 (2014). https://doi.org/10.1016/j.ceramint.2014.03.128
42. Pastero, L.; Bruno, M.; Aquilano, D.: About the genetic mechanisms of apatites: a survey on the methodological approaches. Minerals **7**(8), 139 (2017). https://doi.org/10.3390/min7080139
43. Joshi, D.; Maurya, N.K.; Kumar, N.; Mandal, A.: Experimental investigation of silica nanoparticle assisted surfactant and polymer systems for enhanced oil recovery. J. Pet. Sci. Eng. **216**(May), 110791 (2022). https://doi.org/10.1016/j.petrol.2022.110791
44. Oseh, J.O., et al.: Geoenergy science and engineering rheological and filtration control performance of water-based drilling muds at different temperatures and salt contaminants using surfactant-assisted novel nanohydroxyapatite. Geoenergy Sci. Eng. **228**(May), 211994 (2023). https://doi.org/10.1016/j.geoen.2023.211994
45. Ngouangna, E.N.; Manan, M.A.; Oseh, J.O.; Norddin, M.N.A.M.; Agi, A.; Gbadamosi, A.O.: Influence of (3–Aminopropyl) triethoxysilane on silica nanoparticle for enhanced oil recovery. J. Mol. Liquids **315**, 113740 (2020). https://doi.org/10.1016/j.molliq.2020.113740
46. Oseh, J.O., et al.: Synergistic application of polypropylene and silica nanoparticle modified by (3-Aminopropyl) triethoxysilane for cuttings transport. J. King Saud Univ.-Eng. Sci. (2020). https://doi.org/10.1016/j.jksues.2020.10.007
47. Gbadamosi, A.O.; Junin, R.; Manan, M.A.; Agi, A.; Yusuff, A.S.: An overview of chemical enhanced oil recovery: recent advances and prospects. Int. Nano Lett. **9**(3), 171–202 (2019). https://doi.org/10.1007/s40089-019-0272-8
48. Imuetinyan, H.; Agi, A.; Gbadamosi, A.; Junin, R.; Oseh, J.: Oil-water interfacial tension, wettability alteration and foaming studies of natural surfactant extracted from Vernonia Amygdalina. Pet. Res. **7**(3), 350–356 (2022). https://doi.org/10.1016/j.ptlrs.2021.12.006
49. Oseh, J.O., et al.: Enhanced cuttings transport efficiency of water-based muds using (3–Aminopropyl) triethoxysilane on polypropylene-nanosilica composite. Arab. J. Chem. **13**(8), 6904–6920 (2020). https://doi.org/10.1016/j.arabjc.2020.07.004
50. El Boujaady, H.; Mourabet, M.; EL Rhilassi, A.; Bennani-Ziatni, M.; El Hamri, R.; Taitai, A.: Adsorption of a textile dye on synthesized calcium deficient hydroxyapatite (CDHAp): kinetic and thermodynamic studies. J. Mater. Environ. Sci. **7**(11), 4049–4063 (2016)
51. Bouropoulos, N.; Stampolakis, A.; Mouzakis, D.E.: Dynamic mechanical properties of calcium alginate-hydroxyapatite nanocomposite hydrogels. Sci. Adv. Mater. **2**(2), 239–242 (2010). https://doi.org/10.1166/sam.2010.1092
52. Rao, D.V., et al.: Synchrotron-based XRD from rat bone of different age groups. Mater. Sci. Eng., C **74**, 207–218 (2017). https://doi.org/10.1016/j.msec.2016.11.136
53. Sharma, M.; Nagar, R.; Meena, V.K.; Singh, S.: Electro-deposition of bactericidal and corrosion-resistant hydroxyapatite nanoslabs. RSC Adv. **9**(20), 11170–11178 (2019). https://doi.org/10.1039/C9RA00811J
54. Londoño-Restrepo, S.M.; Jeronimo-Cruz, R.; Millán-Malo, B.M.; Rivera-Muñoz, E.M.; Rodriguez-García, M.E.: Effect of the nano crystal size on the X-ray diffraction patterns of biogenic hydroxyapatite from human, bovine, and porcine bones. Sci. Rep. **9**(1), 1–12 (2019). https://doi.org/10.1038/s41598-019-42269-9
55. Yekeen, N.; Padmanabhan, E.; Idris, A.K.: Synergistic effects of nanoparticles and surfactants on n-decane-water interfacial tension and bulk foam stability at high temperature. J. Petrol. Sci. Eng. **179**(May), 814–830 (2019). https://doi.org/10.1016/j.petrol.2019.04.109
56. Mohammed, I.; Afagwu, C.C.; Adjei, S.; Kadafur, I.B.; Jamal, M.S.; Awotunde, A.A.: A review on polymer, gas, surfactant and nanoparticle adsorption modeling in porous media. Oil Gas Sci. Technol. **75**, 77 (2020). https://doi.org/10.2516/ogst/2020063
57. Abbas, A., Wan Sulaiman, W. R., Zaidi, J., Agi, A.: Anionic surfactant adsorption: insight for enhanced oil recover. Recent Adv. Petrochem. Sci. 1(5) (2017). Doi: https://doi.org/10.19080/rapsci.2017.01.555574.
58. Zargartalebi, M.; Barati, N.; Kharrat, R.: Influences of hydrophilic and hydrophobic silica nanoparticles on anionic surfactant properties: interfacial and adsorption behaviors. J. Petrol. Sci. Eng. **119**, 36–43 (2014). https://doi.org/10.1016/j.petrol.2014.04.010
59. Rezvani, H.; Riazi, M.; Tabaei, M.; Kazemzadeh, Y.; Sharifi, M.: Experimental investigation of interfacial properties in the EOR

mechanisms by the novel synthesized Fe_3O_4@Chitosan nanocomposites. Colloids Surf., A **544**(January), 15–27 (2018). https://doi.org/10.1016/j.colsurfa.2018.02.012
60. Sheikholeslami, M.: CuO-water nanofluid flow due to magnetic field inside a porous media considering Brownian motion. J. Mol. Liq. **249**, 921–929 (2018). https://doi.org/10.1016/j.molliq.2017.11.118
61. Rahbari, A.; Fakour, M.; Hamzehnezhad, A.; Vakilabadi, M.A.; Ganji, D.D.: Heat transfer and fluid flow of blood with nanoparticles through porous vessels in a magnetic field: a quasi-one dimensional analytical approach. Math. Biosci. **283**, 28–47 (2017). https://doi.org/10.1016/j.mbs.2016.11.009
62. Zeeshan; Rasheed, H.U.; Khan, W.; Khan, I.; Alshammari, N.; Hamadneh, N.: Numerical computation of 3D Brownian motion of thin film nanofluid flow of convective heat transfer over a stretchable rotating surface. Sci. Rep. **12**(1), 1–14 (2022). https://doi.org/10.1038/s41598-022-06622-9
63. Liang, Y.; Hilal, N.; Langston, P.; Starov, V.: Interaction forces between colloidal particles in liquid: theory and experiment. Adv. Coll. Interface. Sci. **134–135**, 151–166 (2007). https://doi.org/10.1016/j.cis.2007.04.003
64. Leite, F.L.; Bueno, C.C.; Da Róz, A.L.; Ziemath, E.C.; Oliveira, O.N.: Theoretical models for surface forces and adhesion and their measurement using atomic force microscopy. Int. J. Mol. Sci. **13**(10), 12773–12856 (2012). https://doi.org/10.3390/ijms131012773
65. Li, S.; Torsæter, O.; Lau, H.C.; Hadia, N.J.; Stubbs, L.P.: The impact of nanoparticle adsorption on transport and wettability alteration in water-wet Berea sandstone: an experimental study. Front. Phys. **7**(May), 1–12 (2019). https://doi.org/10.3389/fphy.2019.00074
66. Nguyen, V.; Papavassiliou, D.V.: Hydrodynamic dispersion in porous media and the significance of lagrangian time and space scales. Fluids **5**(2), 79 (2020). https://doi.org/10.3390/fluids5020079
67. Agista, M.N.; Andersen, P.Ø.; Yu, Z.: Modelling nanofluid injection in porous media. J. Pet. Sci. Eng. **176**, 836–849 (2019). https://doi.org/10.1016/j.petrol.2019.02.006
68. Ummul, S., Asema, K., Arif, M., Khan, A., Sheikh, A. A.: Effects of concentration viscometric study of the sodium chloride in ethanol-water mixed system effects of concentration on viscometric study of the sodium chloride in ethanol-water mixed system. no. February, (2016).
69. De Azevedo, B.R.S.; Alvarenga, B.G.; Percebom, A.M.; Aurora, P.: Interplay of interfacial and rheological properties on drainage reduction in CO_2 foam stabilised by surfactant/nanoparticle mixtures in brine. Colloids Interfaces **7**(1), 2 (2023)
70. Kazemzadeh, Y.; Dehdari, B.; Etemadan, Z.; Riazi, M.; Sharifi, M.: Experimental investigation into Fe_3O_4/SiO_2 nanoparticle performance and comparison with other nanofluids in enhanced oil recovery. Pet. Sci. **16**(3), 578–590 (2019). https://doi.org/10.1007/s12182-019-0314-x
71. Bryan, C.R.; Knight, A.W.; Katona, R.M.; Sanchez, A.C.; Schindelholz, E.J.; Schaller, R.F.: Physical and chemical properties of sea salt deliquescent brines as a function of temperature and relative humidity. Sci. Total Environ. **824**, 154462 (2022). https://doi.org/10.1016/j.scitotenv.2022.154462
72. Van Der Spek, D.; Van Arendonk, J.A.M.; Bovenhuis, H.: Genome-wide association study for claw disorders and trimming status in dairy cattle. J. Dairy Sci. **98**(2), 1286–1295 (2015). https://doi.org/10.3168/jds.2014-8302
73. Jeevanandam, J.; Barhoum, A.; Chan, Y.S.; Dufresne, A.; Danquah, M.K.: Review on nanoparticles and nanostructured materials: history, sources, toxicity and regulations. Beilstein J. Nanotechnol. **9**(1), 1050–1074 (2018). https://doi.org/10.3762/bjnano.9.98
74. Sun, X.; Zhang, Y.; Chen, G.; Gai, Z.: Application of nanoparticles in enhanced oil recovery: a critical review of recent progress. Energies **10**(3), 345 (2017). https://doi.org/10.3390/en10030345
75. Babakhani, P.; Bridge, J.; Doong, R.A.; Phenrat, T.: Parameterization and prediction of nanoparticle transport in porous media: a reanalysis using artificial neural network. Water Resour. Res. **53**(6), 4564–4585 (2017). https://doi.org/10.1002/2016WR020358
76. Ngouangna, E.N., et al.: Effect of salinity on hydroxyapatite nanoparticles flooding in enhanced oil recovery: a mechanistic study. ACS Omega (2023). https://doi.org/10.1021/acsomega.3c00695
77. Bila, A.; Torsæter, O.: Article experimental investigation of polymer-coated silica nanoparticles for EOR under harsh reservoir conditions of high temperature and salinity. Nanomaterials **11**(3), 1–17 (2021). https://doi.org/10.3390/nano11030765
78. Adil, M.; Zaid, H.M.; Raza, F.; Agam, M.A.: Experimental evaluation of oil recovery mechanism using a variety of surface-modified silica nanoparticles: role of in-situ surface-modification in oil-wet system. PLoS ONE **15**(7 July), 1–24 (2020). https://doi.org/10.1371/journal.pone.0236837
79. Yu, F., et al.: Dispersion stability of thermal nanofluids. Prog. Nat. Sci.: Mater. Int. **27**(5), 531–542 (2017). https://doi.org/10.1016/j.pnsc.2017.08.010
80. Canillas, M.; Rivero, R.; García-Carrodeguas, R.; Barba, F.; Rodríguez, M.A.: Processing of hydroxyapatite obtained by combustion synthesis. Bol. Soc. Esp. Ceram. Vidrio **56**(5), 237–242 (2017). https://doi.org/10.1016/j.bsecv.2017.05.002
81. Rial, R.; González-durruthy, M.; Liu, Z.; Ruso, J.M.: Advanced materials based on nanosized hydroxyapatite. Molecules **26**(11), 1–22 (2021). https://doi.org/10.3390/molecules26113190
82. Hommel, J.; Class, H.; Coltman, E.: Porosity–permeability relations for evolving pore space: a review with a focus on (bio-) geochemically altered porous media. Transp. Porous Media **124**(2), 589–629 (2018). https://doi.org/10.1007/s11242-018-1086-2
83. Shahzad, M.; Mohamed, K.; Mohammed, M.; Salaheldin, H.; Hussein, I.: Clay minerals damage quantification in sandstone rocks using core flooding and NMR. J. Petrol. Explor. Prod. Technol. **9**(1), 593–603 (2019). https://doi.org/10.1007/s13202-018-0507-7
84. Zou, W.; Zhong, Y.; Vanapalli, S.K.: Effect of montmorillonite content and sodium chloride solution on the residual swelling pressure of an expansive clay. Environ. Earth Sci. **77**(19), 1–12 (2018). https://doi.org/10.1007/s12665-018-7873-9
85. Xu, P.; Zhang, Q.; Qian, H.: Effect of sodium chloride concentration on saturated permeability of remolded loess. Minerals **10**(2), 199 (2020)
86. Jones, F.O.: Influence of chemical composition of water on clay blocking of permeability. J. Pet. Technol. **16**(04), 441–446 (1964)